Calculation of maximum pressure distributions for structural design of a floating wave energy converter

N. Fonseca
nunofonseca@ist.utl.pt

J. Pessoa
joaopessoa@mar.ist.utl.pt

R. Pascoal
rpascoal@mar.ist.utl.pt

Centre for Marine Technology and Engineering (CENTEC)
Technical University of Lisbon, Instituto Superior Técnico
Av. Rovisco Pais, 1049-001 Lisboa - Portugal

T. Morais
tiago.morais@martifer.pt

R. Dias
renato.dias@martifer.pt

Martifer Energia S.A.
Zona Industrial – Apartado 17,
3684-001 Oliveira de Frades, Viseu - Portugal

Abstract

The paper presents an analysis of the maximum pressure loads on the hull of the Martifer Energy WEC. A boundary integral method is used to solve the hydrodynamic problem. The first step consists on validating the numerical results of motions by comparisons with measured experimental data obtained with a scaled model of the WEC. The numerical model is tuned by adjusting the damping of the rotational motions of the device and the equivalent damping of the power take off system.

Then a convergence analysis of the pressure distributions is carried out and the sensitivity of the results with respect to the mesh density and distribution is also assessed. Finally the pressure distributions are calculated for a number of regular waves and also severe irregular sea states. The maximum pressures in irregular seas are represented by probability distributions of maxima.

1. INTRODUCTION

Over the last years there has been a renewed and increasing interest in extracting energy from the waves. Many concepts of wave energy converters (WEC) have been proposed and investigated and some of them reached the prototype phase. Contrary to what occurred with the wind energy sector, where the concepts basically converged to one solution, in the wave energy sector it is still not clear which concepts will prevail. It is likely that several different concepts will become viable, partly depending on site characteristics.

Comprehensive reviews of the state of the art regarding methods of analysis, concepts of WECs and also the technologies involved, can be found in WaveNet [1] and Nielsen et al. [2].

In terms of site location, the WECs can be classified into offshore (deep water), near shore (shallow water) and shoreline devices. Most of the recent concepts consist of near shore floating systems for water depths up to around 100 m, but in average less than this. Near shore seastates are more energetic than shoreline ones, while the offshore sites require more expensive mooring systems and connection to the power grid.

Most of the research effort over the past decades has been focused on the energy capture efficiency and not much on the estimation of structural loads which are important for the survivability of the systems. At present there are no standards or codes available for the structural design of WECs, however, the standards of the Offshore engineering sector are useful for the design of WECs. Recently, the Carbon Trust commissioned Det Norsk Veritas to prepare a 'Guideline on the design and operation of wave energy converters', Carbon Trust [3]. The objective is to provide interpretation and guidance on the application of the various existing standards of the Offshore field.

Additionally, as said before, there are a large variety of concepts of WECs and most of them are still at the development stage, therefore in-service data is still very limited and there are no 'safe' empirical formulas based on previous experience.

For the above reasons, the design wave loads need to be obtained from direct calculations, relying on hydrodynamic models based on first principles together with proper stochastic characterization of the waves.

The structural design of floating wave energy converters is dominated, in most cases, by local loads. Important local loads are those induced by the hydrodynamic pressures on the hull, the forces of the mooring lines at the connecting points to the floater, those resulting from the reaction forces associated to the power take-off system and inertial loads. Global structural loads may also be relevant to design the WECs structural long and slender elements.

This paper focuses on the hydrodynamic pressures applied to the hull of an articulated WEC. The wave body interactions problem is solved in the frequency domain by a boundary integral method. The effects of the power take-off system (PTO) are represented by a simple linear spring-damper model. Due to the characteristics of the WEC, viscous effects influence the vertical motions especially around the natural frequencies of these motions. The coefficients representing the PTO and the linearized viscous effects are calibrated by comparing the numerical predictions with data obtained from an experimental program.

The calibrated model is then used to compute pressure distributions in regular waves and also in irregular severe seastates.

2. FORMULATION

2.1. Green Function Panel Method

Motions and forces on the WEC have been estimated by a standard 3D linear radiation-diffraction flat panel method, which has been applied in the form of the commercial WAMIT package. The mathematical formulation uses variants of the divergence theorem to convert the problem from a volume distribution of sources into a surface integral equation for the source strengths. This equation is classified as a Fredholm integral equation of the second kind.

The method used to solve the integral equation, implemented in WAMIT, uses a Green function which satisfies the radiation condition and all boundary conditions with the exception of the kinematic boundary condition on the body and, as such, the problem is to be solved only across the mean wet surface of the body. The body boundary condition, however, is imposed only on a discrete set of points on the wet surface and the sources distributed on a discrete set of panels, a situation that leads to a matrix equation for the source strength. The solution is found in the frequency domain. Details of the formulation and some numerical aspects can be found in (Lee and Newman [4], Lee [5]).

In this case the body is composed of two rigid parts which are allowed to oscillate relative to each other about a single transverse shaft. Because the body is articulated, there is an additional degree of freedom associated with rotation. The additional degree has been taken into account in this framework by the use of a generalized mode imposed through a .dll function. This function defines the hinged mode kinematic relations between the fore and after rigid bodies, it is programmed in Fortran and the compiled file is called by Wamit.

2.2. Reference Frame and Motions

The reference frame used to go from general vector notation to the specific calculations, has the origin at the intersection of the centre plane with the axis of the hinge mode. X_1 coincides with the intersection of centre plane with the plane which is parallel to the mean waterline and contains the shaft axis, it is positive forward. X_2 coincides with the shaft centre line, and is positive to portside. Finally, X_3 is positive up. All degrees of freedom are sequentially numbered according to standard convention.

It is especially important in this case to have the correct definition of the additional rotation degree of freedom. The additional degree of freedom, x_7, is positive if both bodies close upon each other with downward motion. For kinematic calculations it follows the right hand rule, so it is positive clockwise (right body) and negative otherwise.

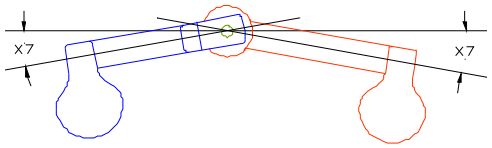

Figure 1 Convention for the additional degree of freedom

2.3. Hydrodynamic Pressures in Harmonic Waves

Once the numerical solution is available for the source strengths, effectively the potential and any of its gradients may be evaluated at desired points of the fluid domain, in particular on points of the outer surface of the body which are of interest for structural design. This is done in the frequency domain and thus pressure may be calculated directly for harmonic waves. The problem is linear and, unless stated otherwise, these are values for unit amplitude incident waves.

The pressure head at any point of the body surface in contact with the fluid domain may be found from the non-stationary, irrotational, form of the Bernoulli equation (these are evaluated in the frequency domain but, for simplicity, frequency has been dropped):

$$\bar{p}_{\text{inst}} = -\frac{1}{g}\frac{\partial \phi_t}{\partial t} - x_3 - \left(\vec{r}_{op} \times \vec{\Theta}\right) \cdot \hat{e}_3 \qquad (1.1)$$

where ϕ_t is the total potential, i.e. includes incident, scattered and radiation potentials, x_3 is the linear motion in heave, $\vec{r}_{op}$ is the location of the point where pressure is evaluated with respect to the origin of the motion calculations and $\vec{\Theta}$ is vector of total angular displacements:

$$\vec{\Theta} = \left[x_4, x_5^+, x_6\right]^T \qquad (1.2)$$

with $x_5^+ = x_5 + signum(body) \cdot x_7$ and $body = -1$ if the point belongs to the aft body and 1 if it belongs to the fore. All motion variables and potentials are complex valued, in which case phase angles are naturally and easily retained.

Because the main objective is to provide pressures for structural design of the outer shell and reinforcements, not only are external pressures of interest but also internal pressures.

The WEC structure has several ballast tanks full of sea water and they are subject to acceleration. Though it is possible to perform full potential theory calculation for these tanks, the pressure gradient has been assumed to result from uniform acceleration. Equilibrium dictates that in such a situation the gradient of the pressure is:

$$\nabla p_{\text{int}} = \rho_{sw}\left(\vec{g} - \vec{a}\right) \qquad (1.3)$$

where ρ_{sw} represents the density of the water, $\vec{g}$ is the acceleration of gravity and $\vec{a}$ is the local acceleration due to the oscillatory motions.

Further, these ballast tanks are located at the ends of the WEC and vertical components of acceleration dominate. Thus, only the vertical component has been integrated (a_z), and the variable part results in the following pressure head:

$$\bar{p}_{\text{int}} = \frac{a_z}{g} h \qquad (1.4)$$

When defining the sign of quantities involved in the final summation, adequate care must be exercised to consider the direction of vectors which are normal to the surface. Inner and outer pressures "subtract" because the vectors associated with the normal stress vector are opposite on opposite sides of the shell, which physically is the correct answer. The total harmonic component of pressure for design is:

$$p_t = p_{\text{inst}} - p_{\text{int}} \qquad (1.5)$$

whose modulus represents the total amplitude and to which the effect of mean hydrostatic pressures, i.e. internal and external, has to be added.

2.4. Hydrodynamic Pressures in Irregular Waves

Once the harmonic components are available and the sea state is defined by its spectral shape, linear calculations for irregular waves are relatively straightforward.
The harmonic components of pressure are for unit amplitude and should be available for an adequate number of frequencies. These in fact constitute transfer functions from elevation to pressure at each point and at positive frequencies (usually only single sided quantities are of interest).
From Fourier analysis one knows that the time varying pressure in irregular waves can be calculated from:

$$\mathrm{Re}\left(F^{-1}\left(p(\omega)\eta(\omega)\right)\right) \qquad (1.6)$$

with single sided long-crested $\eta(\omega)=\sqrt{2S(\omega)d\omega}\cdot e^{i\theta}$, $S(\omega)$ being the wave spectrum and $\theta \sim U[0,\ 2\pi[$ the phase angle. Thus to obtain a time trace, the discrete version of the inverse transform may either rely on the direct use harmonic functions and adequate, discrete $\Delta\omega$ or, if interpolation is performed at uniform frequencies, the faster inverse Fast Fourier Transform. The mean pressure value may be summed at the end.
Because the problem is linear, it is possible to obtain important statistics from the response spectrum. The pressure variance is the area under the pressure spectrum (normalization factors may apply depending on how spectra have been defined, e.g. Meirovitch [6]):

$$\sigma_p^2 = \int P(\omega)d\omega = \int p(\omega)p^*(\omega)S(\omega)d\omega \qquad (1.7)$$

with the * superscript standing for complex conjugate.

3. CALIBRATION OF THE NUMERICAL MODEL

3.1. Characteristics of the WEC

The concept being developed by Martifer SGPS is a floating wave energy converter to be used at near shore locations. It is composed of two bodies connected by a one degree of freedom articulation. The energy is extracted at the articulation by a power take off system based on hydraulics and actuated by the relative motions between the bodies (see Figure 2). The fore floater receives the incident waves.

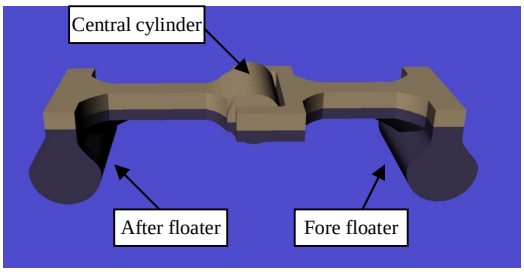

Figure 2 Perspective view of the WEC

The system is moored by a spread mooring that allows the device to weathervane with the wave direction. Different mooring configurations can be used, depending on the site characteristics, however it is a requirement that the mooring is compliant with the wave frequency motions.
Table 1 presents the main characteristics of the device, and, although the total mass is large, a large proportion of it is liquid ballast in the aft and forward cylinders necessary to achieve the design draft and inertial properties. The draft is 14 m while the depth is 17m, therefore most of the device is submerged. This characteristic limits the wave forces in extreme conditions since the largest crests will run over the whole device.

Details of the frequency domain and time domain models for the wave-body interaction of this WEC can be found in Justino et al. [7], while Fonseca et al. [8] presented an analysis of the wave drift forces for the same device.

Table 1: Main characteristics of the WEC

Length overall	Loa (m)	75.0
Length at the waterline	Lwl (m)	68.0
Beam mid	B (m)	24.0
Beam fwd and aft	Bfwd (m)	22.0
Draft	I (m)	14.0
Depth	D (m)	17.0
Free board	FB (m)	3.0
Trim	T (m)	0.0
Angle at the shaft	X7 (º)	0.0
Volume	V (m3)	6603
Displacement	Δ (ton)	6775

3.2. Experimental Program

An experimental program with two models of the WEC of different scales was carried out at the Laboratory of Ship Dynamics of the El Pardo Model Basin in Madrid (Cehipar). The laboratory is made up of three basic facilities: the tank (approximately 150m long and 30m wide), the wave generator and the computerized planar motion carriage. The wave generator is able to produce regular waves, long crested irregular waves and also short crested irregular waves.
The larger model was manufactured at a scale of 1:25 and the objective of the related tests was to assess the dynamic responses of the articulated floater and the efficiency of the power take off system (see figure 2). The tests were carried out in regular waves and irregular waves up to moderate seastates. The scale of the smaller model is 1:40 and the objective of the tests was to investigate the responses in extreme seastates.
The models were manufactured basically in polystyrene and fiber glass, and ballasted to achieve the design displacement, position of the centre of gravity and moments of inertia.

Figure 3 Scaled model during tests in waves

The articulated floater was moored to the stationary carriage by a set of soft spring horizontal mooring lines. The natural period of the horizontal oscillations was much higher than the period of the waves, therefore the horizontal motions are compliant with the wave frequency exciting forces.
The models were instrumented to measure: the absolute motions of the fore floater and the after floater (the two bodies are connected by the articulation), the bending moment, torsional moment and shear force on the shaft of the articulation, and the forces on the mooring lines. For the larger model, several parameters related to the PTO were also measured.
The testing matrix includes regular and irregular waves and different settings off the PTO. Only head waves were considered since the WEC naturally heads to the waves. Head waves travel from the negative to the positive direction of the *x*-axis (see figure 3).

3.3. Geometric Model and Convergence Analysis

To ensure the geometry's panel distribution is sufficiently refined for the numerical code to produce accurate results, one must first perform a convergence analysis. With appropriate software, several panel distributions were created and tested for the WEC's geometry. Since what is needed as a result is the pressure field on the geometry's surface, which is dependent on the fluid's velocity, a finer mesh than usual is required. Some considerations also need to be taken on the way the panels are distributed over the geometry, such as cosine spacing near the free surface and avoiding singularities on the mesh. To evaluate the convergence of the pressure field results, 12 points were selected on especially representative locations, and the pressure transfer functions on those points were analyzed. Based on those results, a mesh with 1520 panels for half a body was selected and can be seen in Figure 4.

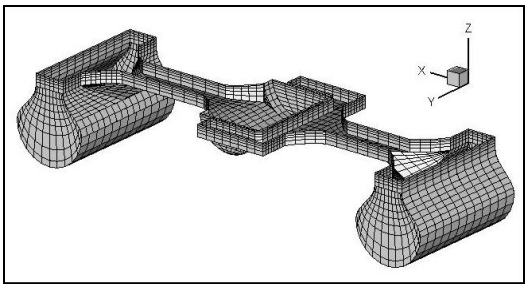

Figure 4 Mesh with 1520 panels for half a body

3.4. Calibration of Numerical Results

The theory behind the numerical method used in this study relies on the linear potential flow assumption, and so it does not account for non linear dissipative effects (like wave breaking) or viscous effects (like skin friction or vortex shedding at sharp corners or around the cylindrical floater). The results obtained from the potential flow numerical method are very accurate for systems where the wave-body interaction forces are dominated by inertial and gravity effects. Due to its particular shape, this WEC will have viscous effects associated to the vertical motions which cannot be neglected, especially around the resonance frequencies.
A possible way around this situation is to introduce additional damping to simulate the viscous effects and see if the numerical results get closer to the experimental ones. Although viscous effects are non linear by nature, due to the use of linear frequency domain representation, they must be introduced in this model as a linear coefficient.
The system in study is different from the more conventional floating structures due to the presence of the PTO. It is necessary to consider not only the viscous damping, but also an additional damping and stiffness to emulate the PTO. This must be done only for the motion mode that actuates the PTO (rotation motion), but it still affects the entire system.
The calibration of numerical results was based on experimental data from regular wave tests performed at basin with a scaled model. The calibration was done in terms of the transfer function amplitude (not accounting for phase) where, by iteratively introducing additional damping and stiffness in the different modes, one fits the numerical results to the experimental ones. In order to make sure that the numerical model is as close to reality as possible, and to reduce the effort in the trial-and-error iterative process to choose the appropriate damping or stiffness, it is necessary to use heuristic knowledge of the physical phenomena involved in the wave-body interaction.
The resulting transfer functions for the calibrated system, as well as the transfer functions for the non calibrated system and the experimental results can be seen in Figure 5 to Figure 8. The additional coefficients derived from the calibration process are presented in Table 2 (right column) together with the potential flow coefficients given for the resonance frequency. The improvement on the accuracy of the model is considerable when the additional coefficients are added.
Some comments are necessary on the empirical correction described in the previous paragraphs and used for the present study.
Starting with the linearized model for the PTO, it is represented by a damping coefficient plus a restoring coefficient, therefore the related forces are linearly proportional to the rotational velocity and displacement. In practice the reaction forces of the PTO are not linear, however it is believed that if the absorbed energy over one wave cycle is the same as the energy dissipated by the numerical linear model over one wave cycle, then dynamic behavior of the WEC is correctly captured and also the indirect effects of the PTO reaction forces on the pressure distribution.
The additional damping coefficient for the rotation, B_{77}, represents a contribution from the PTO and a contribution from additional hydrodynamic effects not accounted for by the linear hydrodynamic model. It is not possible from the experimental data to distinguish one from the other.
Regarding the additional damping coefficients used for the other modes of motion, they are necessary to reduce the numerical transfer function amplitudes around the resonance frequency. Observing the graphs of Figure 5 to Figure 8, it is easy to conclude that the linear potential flow model do not have enough damping to correlate well with the experimental data. In fact, for the frequency range of pitch natural frequency (10s), the potential flow damping is already very small for the different modes of motion (potential damping tends to zero for long

periods). On the other hand it is believed that viscous damping due to flow separation from the fore and after cylinders play an important role. Flow separation is associated to the horizontal and also vertical motions of the cylinders. Table 2 compares the potential flow coefficients, for the 10s period, with the additional "viscous" damping coefficients. The later are of the same order of magnitude for the heave mode, and one order of magnitude higher for the other modes of motion.

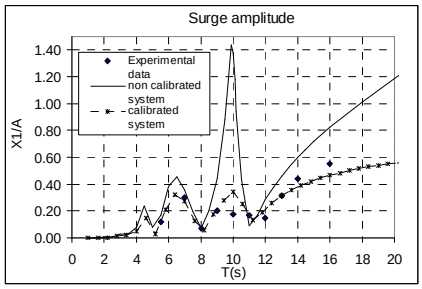

Figure 5 Transfer function for surge amplitude – numerical and experimental results

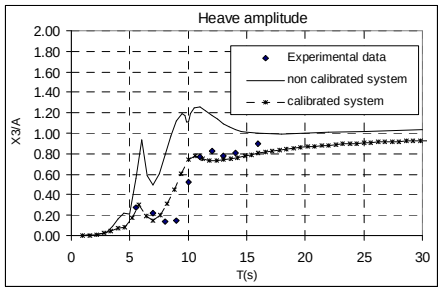

Figure 6 Transfer function for heave amplitude – numerical and experimental results

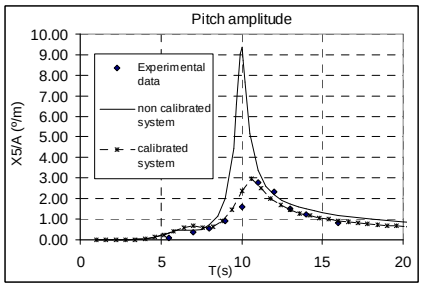

Figure 7 Transfer function for pitch amplitude – numerical and experimental results

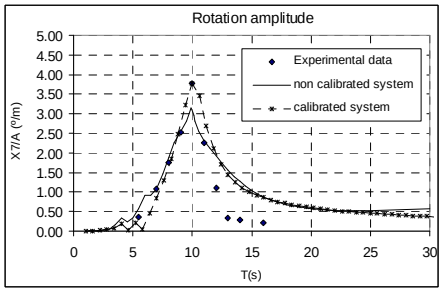

Figure 8 Transfer function for rotation amplitude – numerical and experimental results

Some of this additional damping may be artificial in the sense that nonlinear geometry effects may in part be responsible for the reduction of the experimental resonance peaks compared to the potential flow results. In fact, since the free board of the WEC is small, the deck is easily submerged for finite amplitude incident waves which tend to limit the motion amplitudes.

Returning to the damping associated to viscous effects, it has a direct effect on the pressure distributions because of the vortex shedding and an indirect effect on the pressure distributions since the motions become reduced. The simplified model used here for the viscous effects represents correctly the second, but not the first.

Finally it worth mentioning that the calibration of the numerical model is in principle valid only for the wave amplitudes tested since the additional coefficients in fact represent linearized nonlinear effects.

In spite of the limitations discussed in the previous paragraphs, it is believed that the predicted pressure distributions on the hull of the WEC are realistic.

Table 2 : Potential flow coefficients and additional coefficients derived from the calibration process

Damping Coefficient	Potential flow coefficient	Linearized additional coefficient
B_{11} (N.s/m)	6.37E+05	9.30E+06
B_{33} (N.s/m)	2.10E+06	3.10E+06
B_{55} (N.m.s)	1.20E+07	3.30E+08
B_{77} (N.m.s)	3.98E+08	1.21E+09

Restoring Coefficient	Hydrostatic	PTO
K_{77ad} (N.m/rad)	2.90E+09	7.80E+08

4. PRESSURE DISTRIBUTIONS IN REGULAR WAVES

This section presents selected results of the pressures in harmonic waves. The different components contributing to the total pressure are discussed. The first sub-section focuses on pressure distributions on the mean hull wetted surface for one specific wave frequency, while the second one presents transfer functions for two points on the hull surface.

4.1. Qualitative Analysis of Pressure Distributions

The total pressure is divided and calculated in 5 parts, namely:

(a) Hydrodynamic component, which includes the pressure contributions from the incident and diffracted waves and from the radiated waves due to the motions of the WEC;

(b) Time dependent hydrostatic component which depends of the variation of vertical position of the point where the pressure is being calculated with respect to its mean position;

(c) Interior dynamic component dependent on the WECs acceleration and associated to the ballast tanks, which are considered to be completely full and thus with no interior free surface effects;

(d) Exterior mean hydrostatic component, which is the hydrostatic pressure for the equilibrium position of the WEC;

(e) Interior hydrostatic component associated to the ballast tanks and dependent only on the distance from the point where the pressure is calculated to the top of the tank.

The first 3 components are dynamic and linearly proportional to the wave amplitude, and in regular waves they are harmonically time dependent. Taking into account the phases of each component, and adding these components together one obtains the dynamic component of the total pressure. For the hydrostatic steady components (d and e) it is only needed to notice that they are opposite to each other, and the addition of these will result in the hydrostatic mean component of the total pressure.

So that the order of magnitude of each of these components is made clearer, some figures are presented which contain the pressure components distribution over the WEC mean hull wetted surface in regular waves. The results are for 1m wave amplitude and the harmonic wave period corresponding to the rotation motion resonance (10s). The results are presented in a scale of pressure head in meters (normalized by the wave amplitude).

Figure 9 presents the hydrodynamic pressure distribution, meaning the component associated to the sum of incident, diffracted and radiation effects. Different plots correspond to different instants within one wave cycle, where t/T=0 corresponds to the wave crest at the middle of the articulated floater. Waves travel from the negative to the positive direction of the longitudinal axis.

Figure 10 presents distributions of different components of the pressure, all for the time instant when the hydrodynamic component is maximum at the floater side receiving the incident waves, namely the fore floater (t/T=0.75). Different plots correspond, from top to bottom to: hydrodynamic component, time dependent component of the hydrostatic outside pressure, mean hydrostatic pressure given by the difference between the outside and inside ballast tank mean components, dynamic component of the ballast tanks pressure and, finally, the total pressure on the mean hull wetted surface given by the difference between the ballast tanks pressures and the total outside pressures.

The hydrodynamic pressure maximum (Figure 9) is felt in frontal area of the WEC, where it first receives the incident wave. It has a value of about 2 m pressure head. Theoretically, for the WEC to absorb power, the radiated wave should interact destructively with the incident wave, and so the combined wave system should have less energy after passing through the WEC. In terms of pressure this means that the interaction between the radiation pressure and the diffraction pressure should be such that the total hydrodynamic pressure is smaller in the posterior part of the WEC, which can be seen in the figure.

The dynamic component of the exterior hydrostatic pressure (Figure 10) is only dependent on the variation of the vertical position of the point where the pressure is calculated, and so it only changes in the longitudinal direction. Its maximum value is felt on the after floater, where the largest vertical motions occur. This result is consistent with the experimental observations, where the after body registered larger movements then the fore body.

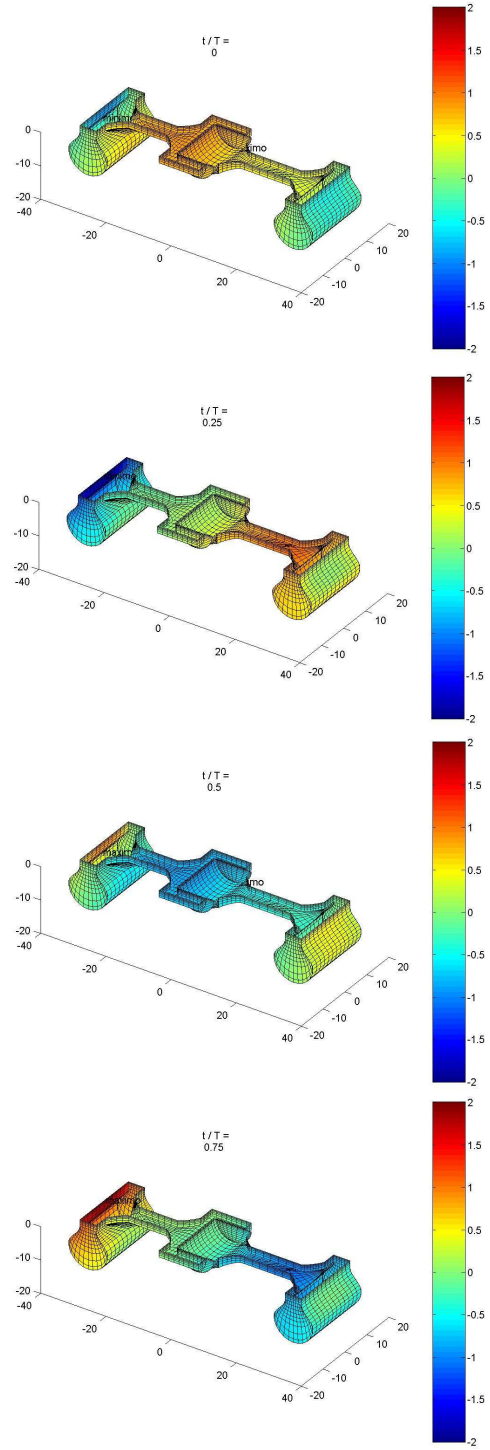

Figure 9 Hydrodynamic pressure for a harmonic wave with of 1m amplitude and a period of 10s

The mean hydrostatic component of the total pressure only changes in the vertical direction up until 14 m .The position of the ballast tanks can be seen in the figure, since that in the areas that are contiguous to them the pressure does not increase with depth. There is a tank in the middle of the fore and of the after cylinder without

ballast, therefore a vertical strip of larger hydrostatic pressure is observed.

The dynamic component of the ballast tanks pressure is associated with the inertial forces of the fluid held in the ballast tanks, and so it only exists on areas which are in contact with such tanks. It only varies in the vertical direction, and even for an incident wave with amplitude of only 1 m it can reach oscillations of up to 1.5 m water column. This maximum is felt at the bottom of the cylinders.

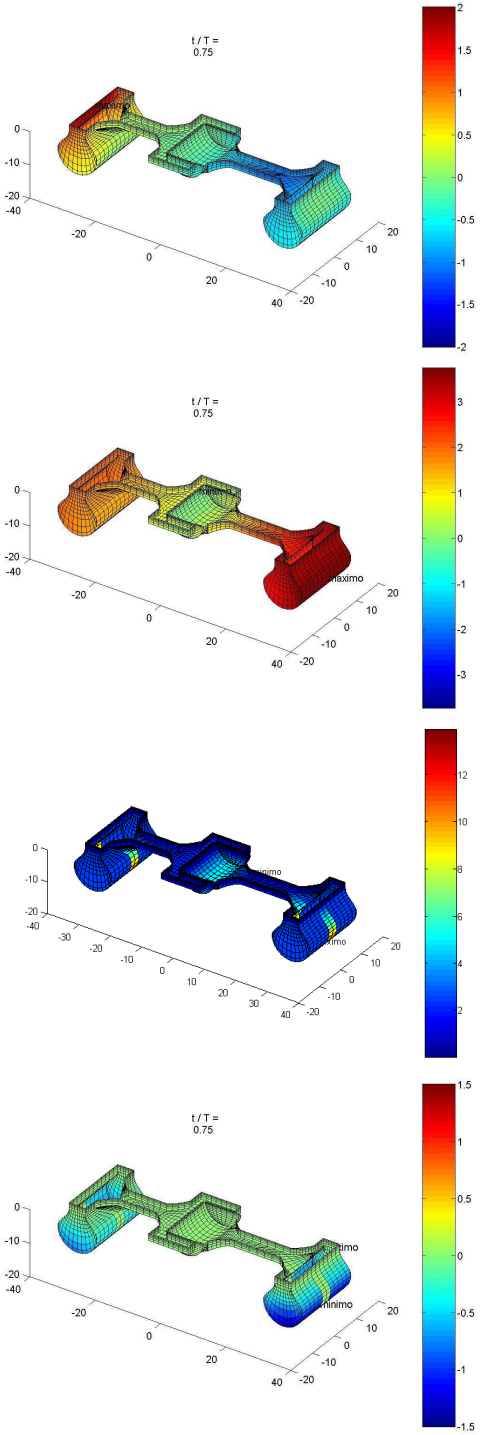

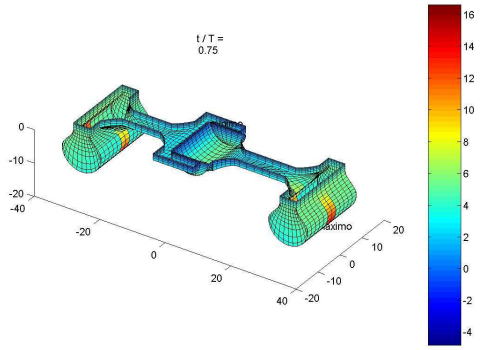

Figure 10 Pressure components for the time instant of maximum hydrodynamic pressure at the forward body. From top to bottom: hydrodynamic, time dependent component of hydrostatic, mean hydrostatic (exterior - interior), interior dynamic, total pressure

The total pressure (bottom Figure 10) for this particular situation oscillates between 16 m water column in the bottom of the fore and after cylinder, around the middle of the cylinders, and 4 m near the free surface. In the bottom areas near the ballast tanks there are very high pressure gradients which will produce high shear forces that will need to be taken into account in the structural design.

4.2. Transfer Functions of Pressures

Figure 11 presents the transfer functions of the pressures at two points of the hull, as function of the wave period. The reference points on the hull are the number 1 and number 7 in Figure 12 and they are on the plane o symmetry of the floater. The first point is at the water line at the side receiving the incident waves, and the second is located in the bottom of the after floater cylinder. The results are given as pressure heads in meters and normalized by the wave amplitude. Each graph includes transfer functions of:

- the total hydrodynamic pressure (incident, diffracted and radiation),
- the dynamic component of the total pressure (hydrodynamic + time dependent component of hydrostatic + ballast dynamic component),
- the time dependent component of the hydrostatic pressure.

One observes in both graphs an amplification of the dynamic components of the pressures around T=10s, which corresponds to the natural period of the rotation motion. The dynamic amplification is much larger for point 1 since the Froude-Krilov and diffracted effects are larger than at the bottom after cylinder where point 7 is located.

Both the hydrodynamic pressure and the hydrostatic time dependent component converge to 1 for long periods. The first indicates that for long waves only the Froude-Krilov component of the hydrodynamic pressure remains, while the second shows that the vertical motion of any point in the body tends to have an amplitude equal to the wave amplitude for long waves. For long waves, the Froude-Krilov and the hydrostatic time dependent pressures tend to cancel each other, which is observed in the line representing the dynamic component of the total pressure.

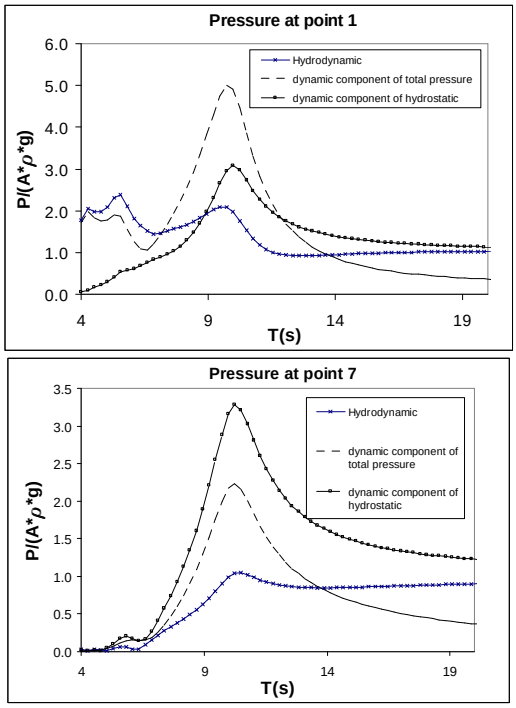

Figure 11 Pressure components transfer functions for 2 selected points

5. PRESSURE DISTRIBUTIONS IN IRREGULAR WAVES

This section presents results of the pressures in irregular seastates. The seastates considered for numerical calculations include operational conditions and extreme conditions and these conditions correspond to the seastates tested at Basin.

As before, the total pressure is composed by the direct sum of the total dynamic pressure and the mean hydrostatic pressure. The first is given by the contributions of the hydrodynamic component, time dependent hydrostatic component and ballast dynamic component. The second is given by the difference between the outside and inside ballast mean hydrostatics.

Since it is assumed that the total dynamic pressures are linear with respect to the incident wave amplitude, the pressures distributions in irregular seatates are assessed using the linear spectral theory.

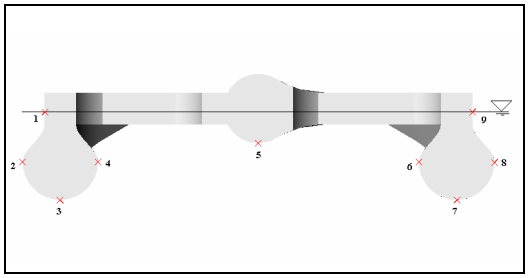

Figure 12 Location of selected points

The first step consists on calculating the variance spectrum of the irregular seastate as function of two parameters, namely the significant wave height (Hs) and the peak wave period (Tp). The JONSWAP spectral shape with a peakness factor of 3.3 is used. Only selected results are presented here in the next sections, starting with response spectra and statistical results of the dynamic pressures for 9 selected points on the hull of the WEC (see Figure 12). All points are located on the plane of symmetry of the body. The points are numbered sequentially from the fore floater (side receiving the incident waves) to the after floater.

5.1. Response Spectra

Figure 13 shows the wave spectra for the most severe seastate tested, with Hs=11m and Tp= 14.5s, and the related response spectra of the total dynamic pressures at the 9 points on the hull. The response spectra present two peaks, the first, occurring at the lower frequency, is related to the peak of the wave spectrum and the second to the natural period of the rotation motion.

Clearly the largest dynamic pressures occur at the fore floater (points 1, 2 and 3), and especially close to the waterline. At the bow and close to the waterline there are simultaneously large vertical motions of the prototype and large dynamic effects due to diffraction of the incident waves. The motions are small near the articulation therefore the dynamic pressures are minimum there (point 5). The pressures increase again on the after floater, basically because the vertical motions are large at this position, however the diffraction effects are small at the stern.

Figure 14 presents the standard deviation of the total dynamic pressure, for four extreme seastates, as function of the points along the length of the articulated prototype. The conclusions are similar to the ones presented before, namely, the pressure is large at the fore body, reduces for the middle body locations and then increases again at the after body. The most severe seastate is the one with Hs=11m and Tp=14.5s. The maximum expected pressures are estimated for this seastate in the next section.

5.2. Maximum Expected Pressure Distribution

For Offshore structures it has become current practice to use the contour line approach to define the seastate conditions that induce the largest wave structural loads during the operational life of the structure. Basically, a set of severe seastates on the 100-years return period contour of the scatter diagram are chosen as the worst conditions where the structure will operate. Then, three hours simulations are carried out for these seastates, appropriate probability distributions are fitted to the maxima of the responses, and finally the largest expected response in the three hours storms is defined as the design wave load. A similar procedure is used here to determine the largest expected dynamic pressures.

As identified in the previous section, the maximum values of the dynamic pressures occur for a seastate with significant wave height and peak wave period respectively of 11m and 14.5s. Since the pressures are assumed linear with respect to the wave amplitude, and furthermore assuming that the process is narrow banded, then the probability distribution of the maxima of the pressures may be represented by a Rayleigh distribution. Figure 15 presents the Rayleigh distribution for the design storm and the 9 points on the hull, where the horizontal line represents the probability level corresponding to the return period of 3 hours.

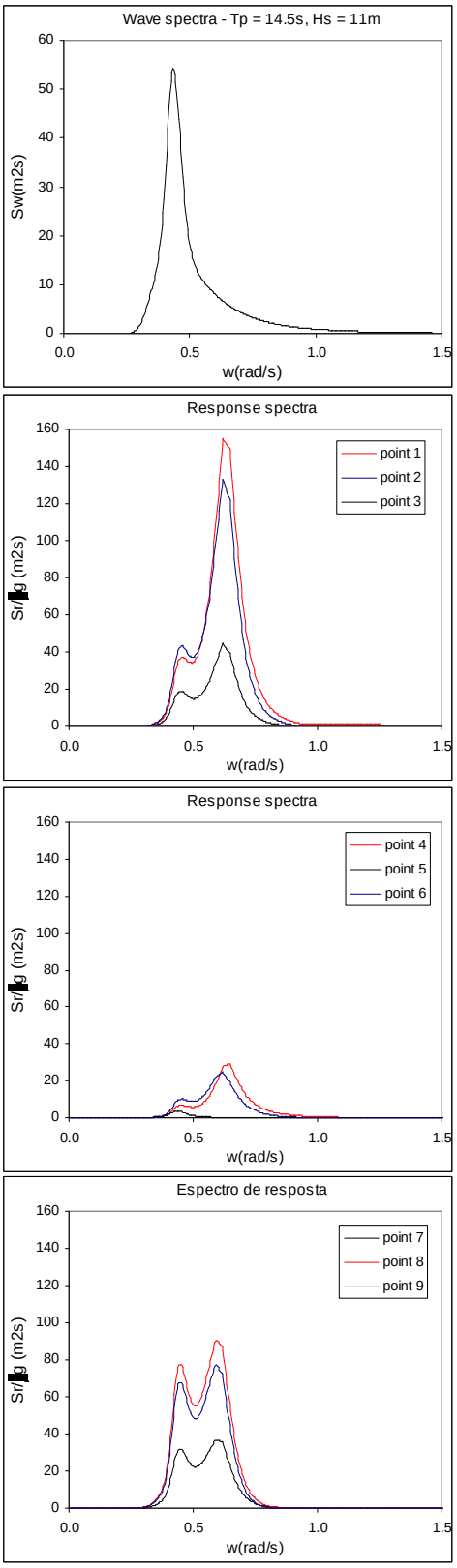

Figure 13 Wave spectra and pressure response spectra for 9 selected points on the hull (Hs=11m, Tp=14.5s)

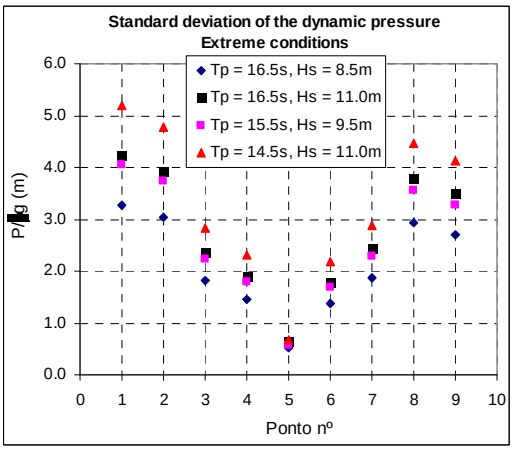

Figure 14 Standard deviation of the dynamic pressure for four extreme seastates

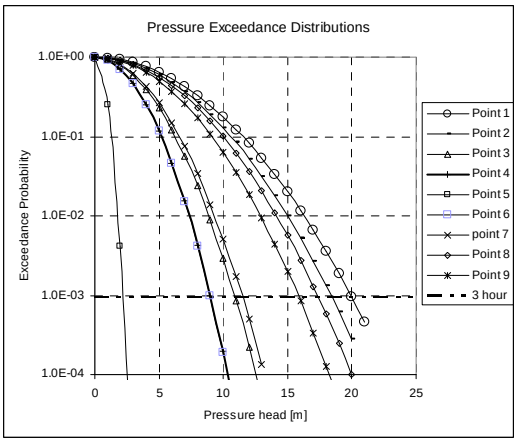

Figure 15 Rayleigh comulative exceedance for pressure.

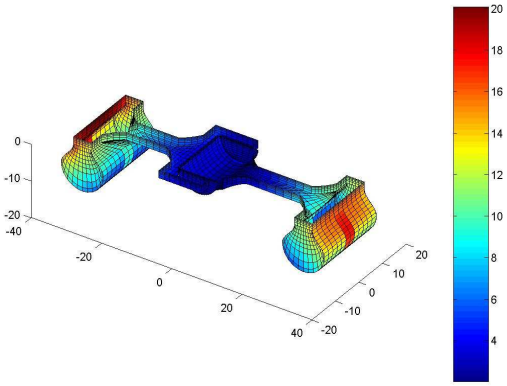

Figure 16 Pressure envelope (only variable part).

The same procedure is repeated for all points of the mesh of the articulated body and then the expected 3 hours maxima are estimated. The result is plotted in Figure 16. This is the time dependent component of the total pressure to which mean hydrostatic values have to be added. The results in Figure 16 represent the map of maximum dynamic pressures that the WEC is expected to suffer during its operational life.

At some points the maximum total dynamic pressure head is almost 20m, to which the mean hydrostatic

pressure must be added. As noticed before, the largest dynamic pressures occur at the floater side receiving the waves (fore floater) and the dynamic pressures are small around the middle of the floater. A strip of large dynamic pressures are observed at the stern cylinder and this part of the floater does not have water ballast inside, therefore the outside dynamic pressures are not opposed by inside dynamic pressures. A similar behavior is obtained for the fore floater cylinder.

6. CONCLUSIONS

A procedure for estimating design wave induced pressure distributions on a WEC has been implemented. It borrows mostly from those already existing for offshore structures with new design and includes special care for inner pressures in ballast tanks, potentially leading to a reduction of local maximum loads.

Since the shape and function of this WEC is quite different from that of existing floating structures, there is a need to rely mostly on solutions with strong physical and mathematical background. These solutions provide a comprehensive setting upon which calibration may be performed by using data from a small, yet representative, experimental program.

Since this WEC is composed of basic volume elements with the shape of oscillating cylinders, the nonlinear, viscous related, damping may have been wrongly estimated by basin data which imposes Froude scaling. This needs to be proven by prototype scale experiments.

Assuming that the pressures are linear with respect to the wave amplitude, and defining a set of extreme seastates, it is possible to estimate the maximum expected pressures on the hull of the WEC during its operational lifetime.

7. ACKNOWLEDGMENTS

Nuno Ferreira from Martifer Energia is thanked for preparing and supplying the experimental data from the model tests.

The work of the second author was partially financed by Fundação para a Ciência e a Tecnologia (FCT) through contract PTDC/EME-MFE/74590/2006.

8. REFERENCES

[1]. Wavenet, 2003, “Results from the work of the European Thematic Network on Wave Energy”, ERK-CT-1999-2001 2000-2003, European Community.

[2]. Nielsen, F.G., et al., 2006, “Ocean Wind and Wave Energy Utilization”, *Proceedings 16th International Ship and Offshore Structures Congress (ISSC’2006)*, Vol. 2, pp. 165-211.

[3]. Carbon Trust, (2005), “Guidelines on the design and operation of wave energy converters” Commissioned by the Carbon Trust and prepared by Det Norske Veritas.

[4]. Lee, C.-H., Newman, J.N., 2004, “Computation of Wave Effects Using the Panel Method”, in Numerical Models in Fluid-Structure Interaction, Preprint, S. Chakrabarti, Ed., WIT Press, Southhampton.

[5]. Lee, C.-H., 2005, “Evaluation of Quadratic Forces Using Control Surfaces”, Report of the 2005 Annual WAMIT Consortium Meeting.

[6]. Meirovitch, L., 1986, *Elements of Vibration Analysis*, McGraw-Hill Intl. Ed.

[7]. Justino, P., Amador, J.C., Morais, T., Hadden, M., Ferreira, N., 2008, “Frequency and time domain models for a two-body wave power device that extracts energy from sea waves by relative pitch motion”, *Proceedings 27th International Conference on Offshore Mechanics and Arctic Engineering (OMAE2007)*, paper OMAE2008-57626, Estoril, Portugal, 15-20 June 2008.

[8]. Fonseca, N., Pascoal, R., Marinho, J. and Morais, T., 2008, “Analysis of wave drift forces on a floating wave energy comverter”, *Proceedings 27th International Conference on Offshore Mechanics and Arctic Engineering (OMAE2007)*, paper OMAE2008-57941, Estoril, Portugal, 15-20 June 2008.